Characterization of atomic spin polarization lifetime of cesium vapor cells with neon buffer gas

Cite as: AIP Advances **8**, 025305 (2018); https://doi.org/10.1063/1.5010294
Submitted: 24 October 2017 . Accepted: 30 January 2018 . Published Online: 08 February 2018

Janet W. Lou, and Geoffrey A. Cranch

Characterization of atomic spin polarization lifetime of cesium vapor cells with neon buffer gas

Janet W. Lou[a] and Geoffrey A. Cranch
Optical Sciences Division, U.S. Naval Research Laboratory, 4555 Overlook Ave., S.W., Washington, DC 20375, USA

(Received 24 October 2017; accepted 30 January 2018; published online 8 February 2018)

The dephasing time of spin-polarized atoms in an atomic vapor cell plays an important role in determining the stability of vapor-cell clocks as well as the sensitivity of optically-pumped magnetometers. The presence of a buffer gas can extend the lifetime of these atoms. Many vapor cell systems operate at a fixed (often elevated) temperature. For ambient temperature operation with no temperature control, it is necessary to characterize the temperature dependence as well. We present a spin-polarization lifetime study of Cesium vapor cells with different buffer gas pressures, and find good agreement with expectations based on the combined effects of wall collisions, spin exchange, and spin destruction. For our (7.5 mm diameter) vapor cells, the lifetime can be increased by two orders of magnitude by introducing Ne buffer gas up to 100 Torr. Additionally, the dependence of the lifetime on temperature is measured (25 - 47 ^{o}C) and simulated for the first time to our knowledge with reasonable agreement. https://doi.org/10.1063/1.5010294

Optically-pumped magnetometry is a promising technique for achieving sub-fT/Hz$^{1/2}$ magnetic field resolutions.[1] Maintaining the coherence of the spin-polarized atoms is essential to obtaining a strong signal. Cesium vapor cells coated with paraffin have been studied and have demonstrated a potential for extended lifetimes.[2–4] Such cells have also been successfully implemented in magnetometers.[5–8] The disadvantages of paraffin-coated cells are that they are difficult to fabricate, incompatible with high temperature (>80 ^{o}C) operation, and paraffin coatings have been implicated in reduced vapor density through absorption of the atoms over time.[9] Operation at elevated temperatures can be beneficial because it increases the vapor density, leading to improved optical interaction. Another method to increase lifetime is to operate in the spin-exchange free regime, where the background magnetic field is near zero.[10–12] However, many applications require operation in the ambient Earth's field. The addition of an inert buffer gas has been experimentally studied for its effect on lifetime[13–17] and also implemented for magnetometers,[18–22] however there are no published validations of experimentally measured lifetimes with analytical models that include temperature dependence.

Ambient environmental conditions require careful consideration of the various dephasing mechanisms. We focus on wall collisions, spin exchange, and spin destruction to understand their contributions to spin depolarization in Cs vapor cells with Ne buffer gas. Using previously published characterizations of diffusion time, spin exchange cross-section, and spin destruction cross-section, a model is compiled to account for these collision types as a function of gas pressures and temperature. Here, lifetimes are characterized using an all-optical magnetometer setup and their magnetic field range of validity is determined. Comparison of measured lifetimes and the expectations based on the model show good agreement.

One commonly used technique for determining the dephasing time of atomic vapors is the modified Franzen method based on polarization rotation,[2] using a pump and probe scheme as shown

[a]Author to whom correspondence should be addressed. Electronic mail: janet.lou@nrl.navy.mil.

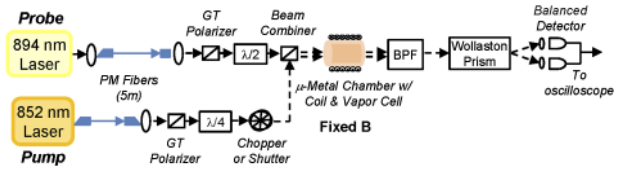

FIG. 1. Setup for measuring the spin coherence lifetimes. PM = polarization-maintaining. BPF = bandpass filter. GT = Glan-Thompson.

in our experimental setup in Fig. 1. The pump laser is locked to the D_2 transition ($S_{1/2}$ (F=4) $\rightarrow$ $P_{3/2}$ (F=4)) and amplitude modulated by either an optical chopper or fast shutter. The probe laser is locked to the D_1 transition ($S_{1/2}$ (F=3) $\rightarrow$ $P_{1/2}$ (F=4)). Both lasers are frequency locked using the DAVLL technique.[23] After launching into free-space from polarization-maintaining fibers, each laser beam passes through a Glan-Thompson polarizer with measured extinction ratio $\geq$23 dB. Then, quartz zero-order waveplates are used to set the input polarizations to the cell. The circularly-polarized pump and linearly-polarized probe are spatially overlapped and pass through the length of the vapor cell. All of the tested vapor cells are manufactured by Precision Glassblowing. The cells are made of Pyrex glass, with 7.5 mm diameter and 2 cm length, and contain a deposit of Cs and optionally filled with Ne buffer gas at a specified room-temperature gas pressure. The cells are placed inside a chamber with three layers of magnetic shielding and a solenoid coil inside the chamber is used to generate a controlled magnetic field parallel to the direction of beam propagation. The pump and probe beam sizes are approximately 5 and 4 mm full-width-at-half-maximum, respectively.

The relaxation measurement technique is based on nonlinear magneto-optical rotation.[24] The polarization of a low-powered probe beam is analyzed by using a Wollaston prism and a balanced amplified detector (ThorLabs PDB210A). With the pump beam blocked, the polarization of the probe beam is initially set so that the two orthogonal polarization signals from the prism are balanced on the detector. When unblocked, the pump beam spin-polarizes the Cs atoms which results in a polarization rotation of the probe. At the output, the pump is removed with a bandpass filter. When the pump is blocked again, the polarized atoms relax and the decay of the induced polarization rotation of the probe is detected and recorded using an oscilloscope. The relaxation time is estimated by fitting the decaying signal (during the pump "off" time period only) to the sum of two exponentials using a nonlinear least-squares method. The equation used for the fitting is of the form $y = a + b\times\exp((x-c)/t_{short}) + d\times\exp((x-c)/t_{long})$, where y is the measured signal, x is the time axis of the signal, and a, b, c, and d are fitting parameters. The shorter time constant, t_{short}, accounts for measurement and system effects such as the transient switch-off time of the pump (*i.e.*, when the pump is not yet fully turned off). The longer time constant, t_{long}, is indicative of the spin-polarization lifetime as measured by the probe beam only.

We measure the lifetime for a range of fixed magnetic fields, using a Cs cell with 37.5 Torr of Ne buffer gas, to ensure accurate characterization for ambient magnetic field strengths. The average pump power is approximately 180 μW (square-wave modulation with 50% duty cycle) and the probe power is approximately 14 μW. The results, shown in Fig. 2, indicate that the estimated lifetimes are relatively constant for the range of Earth's background magnetic field. A similar behavior of a decrease in the measured lifetime at lower fields has been previously reported in Ref. 2. It is suggested that stray fields and magnetic field gradients can effect the lifetime measurements when they are on the same order of magnitude as the applied field.[2] Thus, it is necessary to measure the lifetimes at field levels much higher than the stray fields and gradients. We ensure a background field of at least 10 μT for all subsequent lifetime measurements.

An optically excited atom may lose its spin polarization as a result of collisions. We consider the effects of wall collisions, spin exchange, and spin destruction to estimate the expected lifetime for our vapor cells. The total decay rate is the sum of the decay rates due to each of the mechanisms.

The collision of atoms with the vapor cell walls is one of the primary mechanisms leading to the dephasing of polarized atoms. In a cell without buffer gas, the lifetime is dominated by the transit

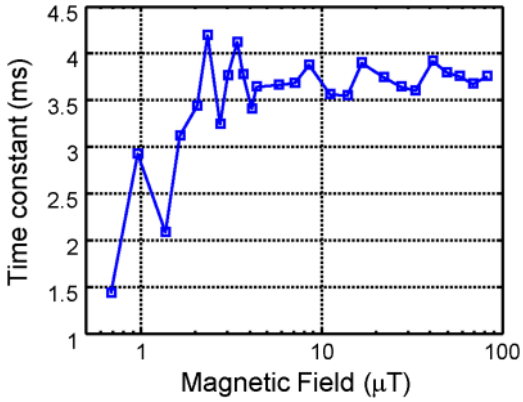

FIG. 2. Measured lifetimes of a Cs with 37.5 Torr Ne buffer gas vapor cell, as a function of DC magnetic field.

time of the Cs to the cell walls. The transit time to the wall is $T_{w,cs} = d/v_{cs}$, where d is the cell diameter and velocity, $v_{cs} = \sqrt{8k_BT/\pi m_{cs}}$, where k_B is Boltzman's constant, m_{cs} is the mass of a Cs atom, and T is the temperature.

In the presence of a buffer gas, the transit time becomes dependent on the diffusion time through the buffer gas, and hence, the properties of the buffer gas such as its density and thermal velocity. Several papers have reported experimental measurements of the diffusion rate, D, of Cs atoms in Ne buffer gas. Ref. 25 reports that $D = 0.185$ cm^2/s at 15 °C and 1 atm, while Ref. 16 reports $D = 0.24$ cm^2/s at 26 °C. It is important to recognize that this value is expected to scale as $T^{3/2}$ and inversely with pressure, (*i.e.*, P^{-1}).

Ref. 25 also presents a theoretical equation, $D = \frac{3}{8(n_{cs}+n_{ne})d_{cs-ne}}(\frac{k_BT}{2\pi m_{cs-ne}})^{1/2}$, where $m_{cs\text{-}ne}$ is the reduced mass of the Cs and the Ne atoms, n_{cs} is the density of Cs atoms, n_{ne} is the density of Ne atoms, and $d_{cs-ne} = 0.343$ *nm* is the collision diameter.[25] The atomic density is related to the vapor pressure by the ideal gas law. The vapor pressure of Cs is slightly complicated by the fact that the melting point of Cs is at 28.5 °C. According to Ref. 26, the vapor pressure in the solid phase is $P = 10^{4.711-3999/T}$ while in the liquid phase, it is $P = 10^{4.165-3830/T}$. Thus, the Cs vapor density follows a slightly different temperature dependence depending on the operating temperature.

Ref. 12 gives the equation for the diffusion time to the cell walls as $T_{w,cs\text{-}ne} = (R/\pi)^2/D$, where R is the radius of a spherical cell. To adjust for our cylindrical geometry, we substitute $1/R^2 = 4/9 \times (1/r + 1/L)^2$ based on the equivalence described in Ref. 27, where r is the radius of the cylinder and L is the length. We calculate the transit rate, $(T_{w,cs\text{-}ne})^{-1}$, using each of the values of D mentioned above, as a function of pressure and temperature. For comparison to our measured results, we use the average of these three transit rates and define $T_{w,cs\text{-}ne} = (average\ rate)^{-1}$ for use in our simulation model. Additionally, after each value of D is scaled to its corresponding value at 760 Torr and 20 °C, the average is calculated to be 0.1997 cm^2/s. This compares well to the $D=0.20(1)$ cm^2/s value reported by using a technique based on measuring the distribution of spin-polarized Cs atoms.[28]

Spin-destruction collisions may also occur between atoms. Ref. 29 measured the cross-section for Cs spin-destruction collisions to be $\sigma_{sd,cs} = 2.03\text{x}10^{-20}$ m^2. The time for this dephasing mechanism is $T_{sd,cs} = q/(n_{cs}v_{cs}\sigma_{sd,cs})$, where $q=8$ is the nuclear slow-down factor for high polarization.[30] Again, both the density and velocity are dependent on the temperature. The cross-section, however, is expected to be independent of temperature. Experimentally measured spin destruction cross-section for Cs with Ne is reported in Ref. 29 to be $\sigma_{sd,cs\text{-}ne} = 2\text{x}10^{-27}$ m^2 at 100 °C, and in Ref. 15 to be $\sigma_{sd,cs\text{-}ne} = 5.3\text{x}10^{-28}$ m^2 at 44 °C. The time for spin destruction dephasing, in the presence of Ne buffer gas, must account for both the Cs-Cs and the Cs-Ne collisions. Thus, we use $T_{sd,cs\text{-}ne} = q/(n_{cs}v_{cs}\sigma_{sd,cs} + n_{ne}v_{cs\text{-}ne}\sigma_{sd,cs\text{-}ne})$, where $v_{cs-ne} = \sqrt{8k_BT/\pi m_{cs-ne}}$, for the spin destruction dephasing time for Cs cells with Ne buffer gas.

The cross-section for Cs spin exchange collisions depend inversely on the temperature.[32] We use $\sigma_{se,cs} = 2.05\text{x}10^{-18}$ m^2, reported in Ref. 33 for 500 K and scale appropriately (T^{-1} dependence)

to predict the dephasing cross-section at other temperatures. In the case of added Ne buffer gas, Ref. 31 reports the cross-section to be $\sigma_{se,cs\text{-}ne} = 2.9\text{x}10^{-28}$ m^2 at 100 °C. The rate of spin exchange is defined by $R_{se,cs} = n_{cs}v_{cs}\sigma_{se,cs}$ and $R_{se,cs\text{-}ne} = n_{ne}v_{cs\text{-}ne}\sigma_{se,cs\text{-}ne}$. Additionally, there is a broadening factor related to the precession frequency.[33] For completeness, we rewrite Eqn. 102 from Ref. 24, where $R'_{se,cs}$ and $R'_{se,cs-ne}$ are the larger damped rates corresponding to slow spin exchange:

$$R'_{se,cs} \cong \frac{C+1}{[I]}R_{se,cs} - \frac{C^2-1}{2{f_0}^2[I]^3}R^3_{se,cs}$$

and

$$R'_{se,cs-ne} \cong \frac{C+1}{[I]}R_{se,cs-ne} - \frac{C^2-1}{2{f_0}^2[I]^3}R^3_{se,cs-ne}$$

where $f_0 = \gamma B$, $C = \frac{([I]^3+2)}{3[I]}$, $[I] = 2I+1$, B is the magnetic field strength, and $I=7/2$ is the Cs nuclear spin, and $\gamma = 3.5$ *Hz/nT* is the Cs gyromagnetic factor. Finally, we define the dephasing time due to spin exchange using the equations $T_{se,cs} = 1/R'_{se,cs}$ and $T_{se,cs\text{-}ne} = 1/(R'_{se,cs} + R'_{se,cs\text{-}ne})$, for Cs-only and Cs with Ne vapor cells, respectively.

Different vapor cells filled with Ne buffer gas at various pressures are characterized as a function of probe power at ~23 °C. After passing through the Glan-Thompson polarizer, the linearly-polarized light is rotated with a half-wave plate such that the difference signal from the balanced detector is zeroed. By the nature of a half-wave plate, there are four angles of rotation (spaced 90° apart) that will result in such a balanced signal. Additionally, the angles that are set 180° from each other are effectively the same polarization. Nominally for our measurements, there should be no difference which angle is used. However, we have found that the fitted time constant can be effected by the initial balance of the balanced detector. After launching the probe beam with good linear polarization, it encounters a half-wave plate designed for 905 nm wavelength, two aluminum-coated mirrors, a non-polarizing beam splitter, the vapor cell, and the bandpass filter before reaching the Wollaston

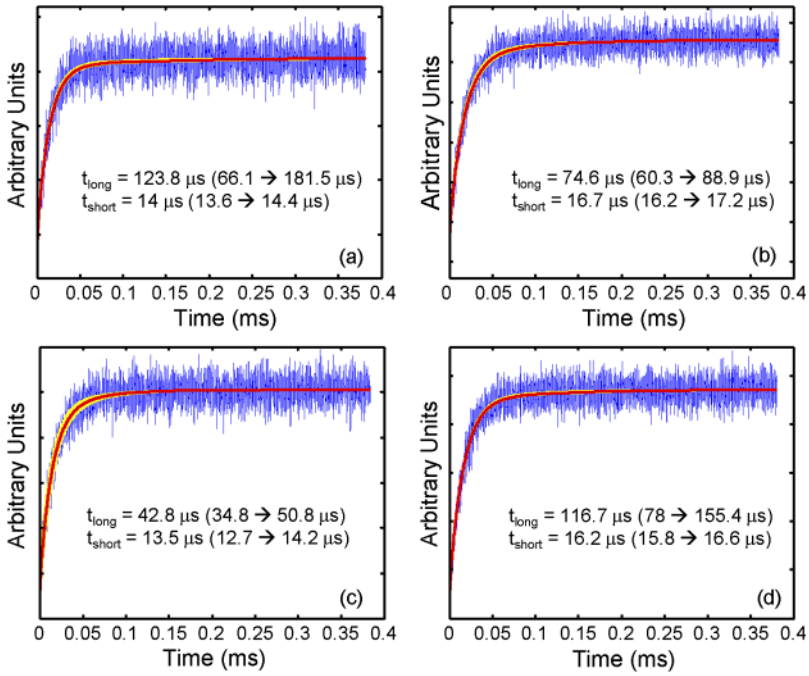

FIG. 3. Examples of measured lifetimes at 23 °C (blue) and fitted results (red) for Cs only vapor cell and probe power ~12 µW, with probe half-wave plate set at (a) 37°, (b) 126°, (c) 216°, and (d) 308°. The uncertainty region defined by the curves corresponding to the simultaneous 95% confidence bounds for both time constants are shown as a (yellow) band around the fitted curve.

prism and detector. Operating at a different wavelength than the design wavelength of the waveplate means that the output beam has some degree of ellipticity. The remaining components may also introduce additional ellipticity to the polarization due to intrinsic birefringence. Thus, it is likely that the polarization of the probe beam is not purely linear inside the vapor cell, and the degree of ellipticity is not obvious from monitoring the balanced detector. In order to obtain the range of values, we rotate the half-wave plate to each of the four "balance points" and record the relaxation signal. Fig. 3 shows examples of our measured decay signals and fitting results for the case of Cs only and ~12 μW probe power, corresponding to each of the four angles. The uncertainty region defined by the curves corresponding to the simultaneous 95% confidence bounds for the two fitted time constants is also shown as a band in Fig. 3. It is clear that a wide range of fitted time constants may be obtained from these cases that are ideally identical. In general, the range defined by the uncertainty of each fit is less than the range obtained for the different waveplate angles, suggesting that the fits are not the limiting error source in our case. Thus, we further explore how an extended collection of measurements may be used to obtain a reasonable estimate of the actual time constant.

All the fitted time constants for a range of probe powers are plotted in Fig. 4. A range of probe powers is tested to ensure that the powers are low enough to minimize self-pumping by the probe beam, but still yield a sufficiently high signal-to-noise ratio to allow a reasonable fit. Ideally, we expect to see little power dependence at these power levels. We find that the variation of the average time constant at each power is small compared to the variation due to the waveplate setting. Note that at the lowest measured power for each cell, there tends to be a greater spread of the fitted time constant as a function of the waveplate angle. This may be an indication of a fitting limitation due to poor signal-to-noise ratio. It is interesting to note that particularly in the 37.5 Torr and 200 Torr cases (Figs. 4c and 4d), the pairs of angles that are 180° offset often resulted, as expected, in similar time constants for each power. For pure Cs, the average measured lifetime is only ~60 μs, dominated by dephasing caused by wall collisions. With the addition of Ne buffer gas, the lifetime increases for increasing buffer gas pressure due to the increased diffusion time. For 10, 37.5, and 200 Torr Ne, the average of all the fitted time constants shown in Fig. 4 for the respective pressures are approximately 1.1 ms, 2.8 ms, and 13.8 ms.

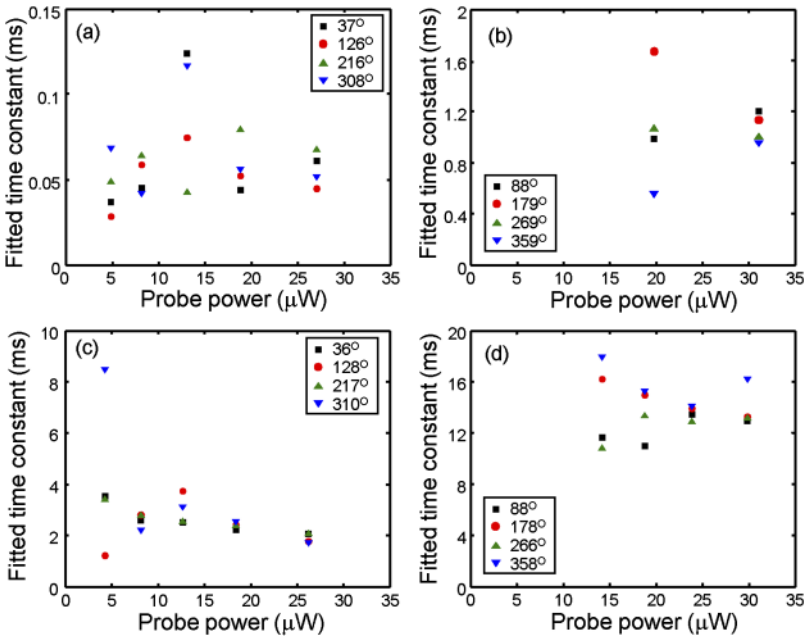

FIG. 4. Measured lifetimes at 23 °C for (a) Cs only, (b) Cs with 10 Torr Ne, (c) Cs with 37.5 Torr Ne, and (d) Cs with 200 Torr Ne, as a function of probe power. For each power, the spin-polarization lifetime is characterized with the half-wave plate set to each of the four angles where the probe beam is initially balanced on the detector.

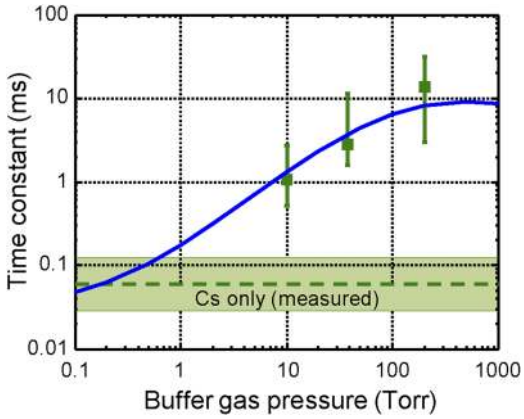

FIG. 5. Calculated lifetime expectations (solid blue line) as a function of buffer gas pressure at 23 °C. The green squares are the average measured results, with the error bars indicating the full range of fitted values obtained as shown in Fig. 4. The green dashed line is the measured result and the shaded band indicates the full range of fitted values for the pure Cs (no buffer gas) vapor cell.

The average measured lifetimes listed above are plotted in Fig. 5 along with the modeled results based on the equations described above. The full range of fitted time constants are also shown as error bars for the buffer gas cases, and as a colored band for the no buffer gas case. While the overall range of fitted time constants appear relatively large, the dependence of the average value tracks well with expectations. For 10, 37.5, and 200 Torr Ne, the model yielded time constants of approximately 1.3 ms, 3.7 ms, and 8.2 ms, respectively. For the case of pure Cs, the expected time constant is ~34 μs. While our average measured value is higher than this, the expected value falls within the range of our measured values. It is also possible that for such a short time constant, we may be near our measurement limit, leading to a relatively large range for the measured results. In the limit of low pressure (~0.25 Torr), the lifetime tends towards the expected value for pure Cs due to the thermal velocity. As the buffer gas pressure is increased, the lifetime is still dominated by the wall collision effect but increases by two orders of magnitude between ~0.25 Torr and ~100 Torr. At greater than ~100 Torr pressure, the spin exchange effect limits the lifetime to approximately 10 ms. This is comparable to the reported lifetimes from Refs. 2 and 3, when scaled to our cell size, which suggest that a paraffin-coated cell of a similar size should exhibit a lifetime of approximately 20 ms. The measured results match the expected dependence on buffer gas pressure. For the lower pressures where the wall collision effect dominates, our average measured lifetimes are lower than expected. One possible explanation is that because the optical probe beam size is smaller than the cell diameter, an atom that transits out of the optical beam no longer contributes to the measured signal. The spin polarization of that atom is effectively depolarized even before reaching the cell wall.

The spin-polarization lifetime for the case of a cell with Cs and 37.5 Torr Ne buffer gas is measured as a function of temperature. The vapor cell is wrapped with Ni-Cr wire and a DC current is used to heat the cell to the test temperature. Then, the DC current is turned off and the spin-polarization lifetime is optically characterized. The temperature is monitored using a K-type thermocouple placed in contact with the outside of the cell, midway along its length. The temperature variation over the measurement time is no more than 0.3 °C. This characterization is repeated as the cell cools from the warmest temperature. The DC current to the Ni-Cr wire heater is never turned on during the cooling phase. Both datasets are shown in Fig. 6, showing good repeatability with no significant difference between increasing versus decreasing temperature measurements. The theoretical values based on the model described above are also plotted in Fig. 6. The theory and measured data appear to be a reasonable match for temperatures >32 °C. One possible cause for the over-estimation at lower temperatures, where the dephasing is dominated by wall collisions, is the inherent assumption of the wall transit time. The calculations assume a uniform transit time from the center of the cell. However, if our optical beam is not precisely at the center of the cell, and because we have a relatively large

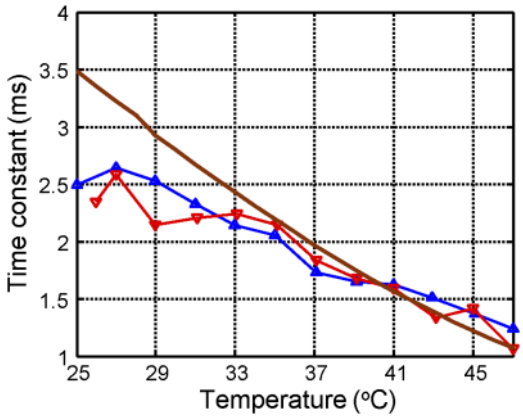

FIG. 6. Measured lifetimes vs. temperature for Cs with 37.5 Torr Ne buffer gas (triangles) vapor cell. The red ∇ (blue Δ) data curve is for decreasing (increasing) temperature. The solid brown line is the calculated expectation.

beam compared to the cell diameter where atoms may be pumped close to the wall, the transit time to the wall may be shorter than the modeled case. As mentioned earlier, transit out of the probe beam may also appear as if the atom has depolarized before reaching the cell wall. We note that the initial test results for the same vapor cell at room temperature, shown in Fig. 2, indicate lifetimes between 3.5 and 4 ms, which is more consistent with the calculations. This closer agreement may be explained by improved alignment of the pump and probe beams to the cell for the measurements in Fig. 2. For temperatures above 32 °C, the spin exchange effect dominates over the wall collision effect in this cell.

In summary, the dephasing time of optically-pumped Cs atoms in confined vapor cells with Ne buffer gas has been characterized. Pressure and temperature dependences are included in comparisons to expectations based on published values for collision cross-sections and diffusion rates. The dependence of the lifetime on buffer gas pressure is in good agreement with expectations. For our cell size of 7.5 mm diameter and 2 cm length, the lifetime is dominated by the wall collision effect at low pressure to tens of microseconds. As buffer gas pressure increases between ~0.25 Torr and ~100 Torr, the lifetime is expected to increase by two orders of magnitude. At greater than ~100 Torr pressure, the spin exchange effect dominates over the wall collisions effect and limit the lifetime to approximately 10 ms. Additionally, the dependence of the lifetime on temperature is measured and compared with theory for the first time to our knowledge. The theoretical expectations over-estimate the measured lifetime in the region dominated by wall collisions, but matched well for higher temperatures where spin exchange dominated. Optical alignment and transit of atoms out of the optical beams may explain this discrepancy. These calculations may be used to predict the performance of Cs vapor magnetometers operating in ambient environments.

This work was supported by the Office of Naval Research.

[1] D. Budker and M. Romalis, Nat. Phys. **3**, 227 (2007).
[2] M. T. Graf, D. F. Kimball, S. M. Rochester, K. Kerner, C. Wong, and D. Budker, Phys. Rev. A **72**, 023401 (2005).
[3] G. DiDomenico, H. Saudan, G. Bison, P. Knowles, and A. Weis, Phys. Rev. A **76**, 023407 (2007).
[4] W. Chalupczak, R. M. Godun, P. Anielski, A. Wojciechowski, S. Pustelny, and W. Gawlik, Phys. Rev. A **85**, 043402 (2012).
[5] W. Li, P. Lin, X. Peng, and H. Guo, in *Proc. of Conf. on Lasers Electro-Opt., San Jose, CA, USA, 2014* (IEEE, 2014), Paper JW2A.131.
[6] M. V. Balabas, D. Budker, J. Kitching, P. D. D. Schwindt, and J. E. Stalnaker, J. Opt. Soc. Am. B **23**, 1001 (2006).
[7] H. Ravishankar, S. R. Chanu, and V. Natarajan, Europhys. Lett. **94**, 53002 (2011).
[8] I. Mateos, B. Patton, E. Zhivan, D. Budker, D. Wurm, and J. Ramos-Castro, Sens. and Actuators A **224**, 147 (2015).
[9] E. B. Alexandrov, M. V. Balabas, D. Budker, D. English, D. F. Kimball, C.-H. Li, and V. V. Yashchuk, Phys. Rev. A **66**, 042903 (2002).
[10] J. Fang, R. Li, L. Duan, Y. Chen, and W. Quan, Rev. Sci. Instr. **86**, 073116 (2015).
[11] M. P. Ledbetter, I. M. Savukov, V. M. Acosta, and D. Budker, Phys. Rev. A **77**, 033408 (2008).
[12] J. C. Allread, R. N. Lyman, T. W. Kornak, and M. V. Romalis, Phys. Rev. Lett. **89**, 130801 (2002).
[13] R. Kawabata, K. Fukuda, and A. Kandori, Jap. J. Appl. Phys. **49**, 082401 (2010).
[14] S. Brandt, A. Nagel, R. Wynands, and D. Meschede, Phys. Rev. A **56**, R1063 (1997).
[15] F. A. Franz and E. Luscher, Phys. Rev. **135**, A582 (1964).

[16] S. Legowski, J. Chem. Phys. **41**, 1313 (1964).
[17] J. Kitching, S. Knappe, and L. Hollberg, Appl. Phys. Lett. **81**, 553 (2002).
[18] J.-H. Zhang, Q. Liu, X.-J. Zeng, J.-X. Li, and W.-M. Sun, Chin. Phys. Lett. **29**, 068501 (2012).
[19] J. W. Lou and G. A. Cranch, in *Proc. of 2017 Joint Europ. Freq. Time Forum & IEEE International Freq. Contr. Symp., Besancon, France, 2017* (IEEE, 2017), C3P–H Paper 1297.
[20] M. Stahler, S. Knappe, C. Affolderbach, W. Kemp, and R. Wyands, Europhys. Lett. **54**, 323 (2001).
[21] R. Jimenez-Martinez, W. C. Griffith, Y.-J. Wang, S. Knappe, J. Kitching, K. Smith, and M. D. Prouty, IEEE Trans. Instru. Meas. **59**, 372 (2010).
[22] V. Schultze, R. Jsselsteijn, T. Scholtes, S. Woetzel, and H.-G. Meyer, Opt. Ex. **20**, 14201 (2012).
[23] K. L. Corwin, Z.-T. Lu, C. F. Hand, R. J. Epstein, and C. E. Wieman, Appl. Opt. **37**, 3295 (1998).
[24] D. Budker, D. F. Kimball, S. M. Rochester, V. V. Yashchuk, and M. Zolotorev, Phys. Rev. A **62**, 043403 (2000).
[25] F. A. Franz and C. E. Sooriamoorthi, Phys. Rev. A **10**, 126 (1974).
[26] C. B. Alcock, V. P. Itkin, and M. K. Horrigan, Canadian Metallurgical Quart. **23**, 309 (1984).
[27] E. B. Watson, K. H. Wanser, and K. A. Farley, Geochimica et Cosmochimica Acta **74**, 614 (2010).
[28] D. Giel, G. Hinz, D. Nettels, and A. Weis, Opt. Ex. **6**, 251 (2000).
[29] N. D. Bhaskar, J. Pietras, J. Camparo, W. Happer, and J. Liran, Phys. Rev. Lett. **44**, 930 (1980).
[30] S. Appelt, A. B.-A. Barange, C. J. Erickson, M. V. Romalis, A. R. Young, and W. Happer, Phys. Rev. A **58**, 1412 (1998).
[31] T. G. Walker, Phys. Rev. A **40**, 4959 (1989).
[32] N. W. Ressler, R. H. Sands, and T. E. Stark, Phys. Rev. **184**, 102 (1969).
[33] W. Happer and A. C. Tam, Phys. Rev. A **16**, 1877 (1977).